Applied Mathematical Modelling 100 (2021) 218–239

Contents lists available at ScienceDirect

Applied Mathematical Modelling

journal homepage: www.elsevier.com/locate/apm

Topology- and convexity-preserving image segmentation based on image registration

Daoping Zhang[a], Xue-cheng Tai[b], Lok Ming Lui[a,*]

[a] Department of Mathematics, The Chinese University of Hong Kong, Shatin, Hong Kong
[b] Department of Mathematics, Hong Kong Baptist University, Kowloon Tong, Hong Kong

ARTICLE INFO

Article history:
Received 5 March 2021
Revised 22 July 2021
Accepted 9 August 2021
Available online 17 August 2021

2010 MSC:
68U10
94A08

Keywords:
Registration-based segmentation
Topology- and convexity-preserving segmentation
Level set function
Alternating direction method of multipliers

ABSTRACT

Image segmentation aims to extract the target objects or to identify the corresponding boundaries. For corrupted images due to occlusions, obscurities or noises, to get an accurate segmentation result is very difficult. To overcome this issue, the prior information is often introduced and particularly, the convex prior attracts more and more attentions recently. In this paper, we propose a topology- and convexity-preserving registration-based segmentation model, which can be suitable for both 2D and 3D cases. By incorporating the level set representation and imposing the constraints on the suitable regions, we can explicitly force the fully convex segmentation results or the partially convex segmentation results. To solve the proposed model, we employ the alternating direction method of multipliers and numerical experiments on 2/3D synthetic and real images demonstrate that the proposed model can indeed lead to the accurately topology- and convexity-preserving segmentation.

1. Introduction

The task of image segmentation aims to partition a given image into its constituent objects or to identify the boundaries of target objects. Nowadays, image segmentation, as one of the hottest topics in image analysis and computer vision, attracts more and more attentions and has a wide range of applications [1–4].

Generally, segmentation methods can be divided into two aspects: global segmentation methods and selective segmentation methods. For the global segmentation methods, it aims to segment all the meaningful objects in the given image. One of the most classical global segmentation methods is the Mumford-Shah model [5], a region-based model, which is to compute optimal piecewise-smooth or piecewise-constant approximations of the given image. By adopting the level set function to represent the boundaries of the objects and introducing the Heaviside function and the one-dimensional Dirac measure, the Chan-Vese model is proposed in [6] to solve the piecewise-constant Mumford-Shah model. Furthermore, the Chan-Vese model has been extended to cope with different situations, such as vector-valued images [7], textured images [8], and multiple objects segmentation [9,10]. Since these models are nonconvex, this means that the solution may be different and depends on the locations of the initial guesses. To deal with this difficulty, [11] discusses how the Chan-Vese model can be reformulated as a convex model under some certain conditions. Another kind of the global segmentation methods is snakes [12], an edge-based model, which deforms a parametric curve based on the internal and external forces to locate

* Corresponding author.
E-mail addresses: dpzhang@math.cuhk.edu.hk (D. Zhang), xuechengtai@hkbu.edu.hk (X.-c. Tai), lmlui@math.cuhk.edu.hk (L.M. Lui).

https://doi.org/10.1016/j.apm.2021.08.017
0307-904X/

the boundaries of the target objects. In addition, [13] proposes a geodesic active contour model which allows the topology changes of the evolving curves and [14] introduces a vector field convolution as a new external force to improve the robustness with respect to the noise. For the selective segmentation methods, it is just to segment some particular objects rather than all the objects. By combining the geodesic active contour with the geometric constraint and interpolation, a selective segmentation model is proposed in [15]. Further, to improve the robustness, [16] introduces an intensity-based constraint. More recently, [17] proposes a convex selective model by incorporating an edge-weighted geodesic distance, which allows an arbitrary initialization.

In addition, Convolutional Neural Networks (CNNs) [18] has achieved many successes in many applications. The first CNNs to deal with the image segmentation is Fully Convolutional Networks (FCNs) [19], which is an end-to-end CNN framework. Motivated by FCNs, U-net [20] employs a symmetric structure to concatenate feature maps from different levels together. Recently, [21] proposes a network to segment the salient object in the RGB-D images and [22] devises a network to extract the salient object in the real-time video.

Although there exists many segmentation models, they still may encounter the difficulties in the real applications. For example, when images are degraded by overexposure or underexposure, most intensity-based segmentation models cannot segment the target object accurately as a whole [23]. Also, when the given image is corrupted or obscured, many existing segmentation methods may exclude some crucial parts [24,25]. To make the segmentation results more accurate, it is usually necessary to introduce the prior information about the target objects. In this paper, we mainly consider the convexity shape prior, which is quite common in our daily lives [26].

The convexity-preserving segmentation is to lead to a convex segmentation result, in other words, the resulting segmentation region is convex. Hence, the difficulty is how to ensure that the model can indeed generate a convex segmentation both in theory and in practice. In [27], the authors explicitly model the boundary of the object. By introducing $n \geq 3$ auxiliary surrounding regions, a convex n-polygon can be guaranteed. However, when segmenting a smooth object, n should be large to block the efficiency of the algorithm. A discrete method is proposed in [28], where the constraints on all the straight lines in the discrete image plane are imposed[29]. proposes an image segmentation model based on the L_1 variant of the Euler's elastica energy, which prefers for convex segmentation contours. But since a fourth order nonlinear PDE needs to be solved, the efficient implementation is still a difficulty[26]. proposes a segmentation model by incorporating convexity shape prior using level set representation. This method is based on the observation that the level set function of a convex region must be a convex function. Then [30] extends this idea to the multi-object segmentation. Furthermore, [31] presents a new efficient method for convex shape representation, which is regardless of the dimension of the concerned objects, using level-set approaches.

Recently, there are several works to do the segmentation with the help of image registration, namely, the registration-based segmentation. The foundation of this framework is to build the link between the boundaries of the prior objects and target objects by the resulting transformation. In addition, if the transformation is one-to-one, then the segmentation will be topology-preserving. The advantage of this kind of segmentation method is that the resulting transformation can provide more useful information for some specific applications. In [24], Chan et al. employ the Beltrami representation of a shape to guarantee a topology-preserving segmentation. Further, to get a convex segmentation, [25] combines a specially designed convexity constraint based on the discrete conformality structures of the image mesh with the registration-based segmentation model proposed in [24]. This model can guarantee the segmented region to be fully or partially convex according to the user's preference. However, since the Beltrami coefficient is only defined in complex space, the above mentioned models only can deal with the 2D segmentation. To extend the registration-based segmentation to the 3D case, [23] combines the hyperelastic regularizer with the fitting term in the Chan-Vese model. However, to the best of our knowledge, the 3D convex segmentation based on registration is still not available.

In this paper, we consider combing the registration-based segmentation method with the level set representation to propose a topology- and convexity-preserving registration-based segmentation model, which can be suitable for both 2D and 3D cases. To propose this topology- and convexity-preserving registration-based segmentation model, we need this simple observation: if the transformation y is one-to-one and ϕ is the level set function of $\mathbb{D}$, then $\phi \circ y$ is the level set function of $\tilde{\mathbb{D}}$, where $\tilde{\mathbb{D}} = \{x | y(x) \in \mathbb{D}\}$. Hence, this model can be formulated by imposing an explicit constraint of the level set function to the conventional registration-based segmentation model. To solve the proposed model, we introduce an auxiliary variable and employ the alternating direction method of multipliers (ADMM). Numerical experiments on both 2/3D synthetic and real images demonstrate that the proposed model can indeed lead to the accurately topology- and convexity-preserving segmentation.

Here, we want to emphasize that although our method involves the level set function, it has essential differences from the level set method [26,30,31]. For the level set method [32], it finally aims to find a level set function and for the stability, the process of reinitialization is often unavoidable. Hence, the models in [26,30,31] all constraint the level set function to be a signed distance function. But for our registration-based model, it eventually solves a plausible one-to-one transformation and deforms the initial level set function. In this way, there is no need to force the level set function to be a signed distance function. Furthermore, if we force the deformed level set function to be convex for the whole segmentation domain, it is the fully convex segmentation. Otherwise, a partially convex segmentation can be obtained by restricting the deformed level set function to be convex for some parts of the target domain.

The rest of this paper is organized as follows. In Section 2, some preliminaries used in this paper are reviewed. In Section 3, we propose our topology- and convexity-preserving registration-based segmentation model. Numerical algorithm

is discussed in Section 4 and numerical results are illustrated in Section 5, respectively. Finally, we conclude this paper in Section 6.

2. Preliminaries

In this section, we first review some preliminaries which will be used in this paper. Here, d represents the dimension of the space, which can be 2 or 3.

Definition 1 (Level Set Function, LSF)**.** Let $\mathbb{D}$ be a subset of $\mathbb{R}^d$ and $\partial\mathbb{D}$ be its boundary. A function $\phi : \Omega \subset \mathbb{R}^d \to \mathbb{R}$ is called a level set function of the region $\mathbb{D}$ if it satisfies the following condition:

$$\begin{cases} \phi(x) < 0 & \text{if } x \in \mathbb{D}, \\ \phi(x) = 0 & \text{if } x \in \partial\mathbb{D}, \\ \phi(x) > 0 & \text{if } x \in \Omega\backslash\mathbb{D}, \end{cases} \tag{1}$$

where Ω is the image domain.

Definition 2 (Convex Set [33])**.** A set Ω is a convex set if and only if for any two points $x_1 \in \Omega$ and $x_2 \in \Omega$, we have

$$\alpha x_1 + (1-\alpha)x_2 \in \Omega, \text{ for all } \alpha \in [0,1]. \tag{2}$$

Definition 3 (Convex Function [33])**.** A function ϕ is a convex function if its domain Ω is a convex set and if for any two points $x_1 \in \Omega$ and $x_2 \in \Omega$, the following property is satisfied:

$$\phi(\alpha x_1 + (1-\alpha)x_2) \le \alpha\phi(x_1) + (1-\alpha)\phi(x_2), \text{ for all } \alpha \in [0,1]. \tag{3}$$

Lemma 1 [34]**.** *Assume that ϕ is twice differentiable. Then ϕ is convex if and only if its Hessian is positive semidefinite.*

Theorem 1. *Let a twice differentiable convex function $\phi : \Omega \subset \mathbb{R}^d \to \mathbb{R}$ be a level set function of a region $\mathbb{D}$. Then the region $\mathbb{D}$ is a convex region.*

Proof. For any two points $x_1 \in \mathbb{D}$ and $x_2 \in \mathbb{D}$, we have

$$\phi(\alpha x_1 + (1-\alpha)x_2) \le \alpha\phi(x_1) + (1-\alpha)\phi(x_2) < 0, \text{ for all } \alpha \in [0,1]. \tag{4}$$

Then by the definition of the level set function (Definition 1), we can get

$$\alpha x_1 + (1-\alpha)x_2 \in \mathbb{D}, \text{ for all } \alpha \in [0,1], \tag{5}$$

which shows that the region $\mathbb{D}$ is a convex region. □

3. The topology- and convexity-preserving registration-based segmentation model

In this section, we first review the basic idea of image registration and the registration-based segmentation method. Then we discuss how to combine the level set representation with the registration-based segmentation method to generate a topology- and convexity-preserving segmentation.

3.1. Image registration

Image registration aims to find a plausible transformation to match the corresponding images. Conventionally, two images are given, one as the template $T(x) : \Omega \subset \mathbb{R}^d \to \mathbb{R}$ and the other one as the reference $R(x) : \Omega \subset \mathbb{R}^d \to \mathbb{R}$. To find a transformation $y(x) : \Omega \subset \mathbb{R}^d \to \mathbb{R}^d$ such that the deformed template $T(y(x))$ is similar with the reference $R(x)$ in some sense, the usual way is to minimize the difference for a given measurement, namely, to solve the following variational problem:

$$\min_y \mathcal{D}(T(y(x)), R(x)), \tag{6}$$

where $\mathcal{D}$ is a fitting term. However, just minimizing this fitting term $\mathcal{D}$ is ill-posed because the uniqueness of the solution cannot be ensured [35]. Hence, regularization is indispensable and we can reformulate the variational problem (6) into the following well-posed problem:

$$\min_y \mathcal{D}(T(y(x)), R(x)) + \alpha\mathcal{R}(y), \tag{7}$$

where $\mathcal{R}$ is the regularizer and $\alpha > 0$ is a positive parameter to balance the weight between the fitting term and the regularizer.

There exists many choices for the fitting term [36–39] and in this paper, we only focus on the sum of squared differences (SSD) [39]:

$$\mathcal{D}^{\text{SSD}}(T, R, y) := \frac{1}{2}\int_\Omega (T(y(x)) - R(x))^2 \mathrm{d}x. \tag{8}$$

There also exists many choices for the regularizer [40–52]. Here, we consider the following regularizer proposed in [49]:

$$\mathcal{R}^{\mathrm{QC}}(y) := \frac{\alpha_1}{2}\int_\Omega \|\Delta y\|_{\mathrm{F}}^2 \mathrm{d}x + \alpha_2 \int_\Omega |k(y)|^2 \mathrm{d}x, \tag{9}$$

where $\Delta y = (\Delta y_1, \ldots, \Delta y_d)$, $\|\cdot\|_{\mathrm{F}}$ is the Frobenius norm and $k(y)$ is the conformality distortion defined by

$$k(y) := \begin{cases} \dfrac{1}{d}\dfrac{\|\nabla y\|_{\mathrm{F}}^2}{(\det \nabla y)^{2/d}} & \text{if } \det \nabla y > 0, \\ +\infty & \text{otherwise.} \end{cases} \tag{10}$$

Here, $k(y)$ is the d-dimensional conformality distortion for a mapping y between d-dimensional spaces derived by generalizing the standard conformality distortion defined for mappings between 2-dimensional spaces. This quantity can ensure that the resulting transformation is quasi-conformal and one-to-one.

3.2. Registration-based segmentation method

The registration-based segmentation method is to segment the target objects under the help of the registration skill. To do the image registration, we first need to give a prior image $J(x)$ possessing the same topology structure with the given image $I(x)$ according to the aim of the segmentation. For example, if the given image only has one target object, we can set a simple circle as the prior image. Then after having two images, we can do the registration from two different aspects. The first one is to take the given image as the template and the prior image as the reference. After doing the registration, the ideal situation is that the deformed template can match the reference perfectly, which means that the boundary of the deformed target objects can match the boundary of the priors well. Then we build a link between the boundary of the target objects and the boundary of the priors by the resulting transformation y. Since the priors are prescribed by the user, the location $\hat{x}$ of the boundary of the priors is known. Then we know that the boundary of the target objects is $y(\hat{x})$ and then extract the target objects. The other one is to take the prior image as the template and the given image as the reference. After doing the registration, the deformed prior image can match the input image well. Usually, the prior image is defined by a piecewise-constant function. Then we can just set the threshold to segment the deformed prior image to extract the target objects. In addition, if the resulting transformation y is a one-to-one mapping, it can lead to a topology-preserving segmentation, or in other words, the topological structure of the segmentation result is the same with the topological structure of the prior image.

Next, we build the variational formulations for the registration-based segmentation method from the two aspects mentioned above.

Here, our prior image can be defined as follows:

$$J(c, x) = \begin{cases} c_1, & \text{if } x \in \mathbb{D}_1, \\ \cdots & \\ c_m, & \text{if } x \in \mathbb{D}_m, \end{cases} \tag{11}$$

where m is prescribed by the user, $\Omega = \mathbb{D}_1 \cup \ldots \cup \mathbb{D}_m$ and $\mathbb{D}_i \cap \mathbb{D}_j = \emptyset$, for $1 \le i \ne j \le m$. By introducing the indicator function $\mathcal{X}_\Omega(x)$:

$$\mathcal{X}_\Omega(x) = \begin{cases} 1 \text{ if } x \in \Omega, \\ 0 \text{ if } x \notin \Omega, \end{cases} \tag{12}$$

we can convert (11) into the following equivalent formulation:

$$J(c, x) = \sum_{l=1}^{m} c_l \mathcal{X}_{\mathbb{D}_l}(x). \tag{13}$$

Then, for these two different aspects, variational formulations are shown as follows:

$$\min_{y,c} \mathcal{F}_1(y, c) := \frac{1}{2}\int_\Omega (I(y) - J(c, x))^2 \mathrm{d}x + \mathcal{R}(y) \tag{14}$$

and

$$\min_{y,c} \mathcal{F}_2(y, c) := \frac{1}{2}\int_\Omega (J(c, y) - I(x))^2 \mathrm{d}x + \mathcal{R}(y). \tag{15}$$

The former framework has been used in [23]. But it is difficult to integrate the level set skill to guarantee the convexity-preserving segmentation result. In this paper, we choose the latter framework and in the next subsection, we will discuss how to integrate the level set representation into this framework to obtain the convexity-preserving segmentation model.

3.3. The proposed model

The motivation of our work is based on the following observation: let ϕ be a level set function of $\mathbb{D} = \cup_{l=1}^{m-1}\mathbb{D}_l$, where each $\mathbb{D}_l$ is simply connected and y be a one-to-one mapping, then $\phi \circ y$ is the level set function of $\tilde{\mathbb{D}} = \cup_{l=1}^{m-1}\tilde{\mathbb{D}}_l$, where $\tilde{\mathbb{D}}_l = \{x | y(x) \in \mathbb{D}_l\}$. Assume that each $\tilde{\mathbb{D}}_l$ can be covered by a convex set Ω_l and $\Omega_i \cap \Omega_j = \emptyset$. Hence, if $\phi \circ y$ is twice differentiable and convex with respect to each Ω_l, then according to Theorem 1, we have that each $\tilde{\mathbb{D}}_l$ is convex, which leads to a topology- and convexity-preserving segmentation. Actually, this is the fully convex segmentation model. Further, if Ω_l just covers the part of the boundary of $\tilde{\mathbb{D}}_l$, then it will lead to a partially convex segmentation model. Here, the selection of Ω_l is very flexible and depends on the users.

Based on the above discussion and setting $\bar{\Omega} = \cup_{l=1}^{m-1}\Omega_l$, we propose our topology- and convexity-preserving registration-based segmentation model:

$$\begin{aligned} &\min_{y,c} \mathcal{F}(y,c) := \tfrac{1}{2}\int_\Omega (J(c,y) - I(x))^2 \mathrm{d}x + \tfrac{\alpha_1}{2}\int_\Omega \|\Delta y\|_{\mathrm{F}}^2 \mathrm{d}x + \alpha_2 \int_\Omega |k(y)|^2 \mathrm{d}x \\ &\text{s.t. } \phi \circ y \text{ is convex with respect to } \bar{\Omega}. \end{aligned} \tag{16}$$

Here, ϕ is the level set function of the prior image. Our model (16) gives a transformation y, which deforms the level set function ϕ to another level set function $\phi \circ y$. As a result, the boundary of the target object is given by $\{y^{-1}(x) | x \text{ satisfies } \phi(x) = 0\}$. Hence, unlike the level set method that requires reinitialization [32], there is no need to set ϕ in our model as a sign distance function. For example, if the prior image is a 2D disk, we can employ $\phi(x) = \|x - a\|_2^2 - r^2$ rather than $\phi(x) = \|x - a\|_2 - r$, where a is the center of the disk and r is the radius.

4. Numerical algorithm

In this section, we discuss the details of the numerical algorithm about how to solve the proposed model (16). We consider applying ADMM, which is also used in [31]. Here, since our model does not involve the signed distance function, compared with [31], we only need to introduce one penalty term, which decreases the difficulty of tuning the penalty parameters.

First, by Lemma 1, we can rewrite the proposed model (16) into the following equivalent formulation:

$$\begin{aligned} &\min_{y,c} \mathcal{F}(y,c) := \tfrac{1}{2}\int_\Omega (J(c,y) - I(x))^2 \mathrm{d}x + \tfrac{\alpha_1}{2}\int_\Omega \|\Delta y\|_{\mathrm{F}}^2 \mathrm{d}x + \alpha_2 \int_\Omega |k(y)|^2 \mathrm{d}x \\ &\text{s.t. } \nabla^2(\phi \circ y) \text{ is semidefinite positive with respect to } \bar{\Omega}, \end{aligned} \tag{17}$$

where $\nabla^2(\phi \circ y)$ is the Hessian of $\phi \circ y$. Then, we introduce an auxiliary variable q such that $\nabla^2(\phi \circ y) = q$. Hence, we convert (17) into the following equivalent formulation:

$$\begin{aligned} &\min_{y,c} \mathcal{F}(y,c) := \tfrac{1}{2}\int_\Omega (J(c,y) - I(x))^2 \mathrm{d}x + \tfrac{\alpha_1}{2}\int_\Omega \|\Delta y\|_{\mathrm{F}}^2 \mathrm{d}x + \alpha_2 \int_\Omega |k(y)|^2 \mathrm{d}x \\ &\text{s.t. } \nabla^2(\phi \circ y) = q, \ \ q \text{ is semidefinite positive with respect to } \bar{\Omega}, \end{aligned} \tag{18}$$

Next, denote the set of the semidefinite positive matrices by $\mathcal{C}$ and define an indicator function $\delta_{\mathcal{C}}(q)$:

$$\delta_{\mathcal{C}}(q) = \begin{cases} 0 & \text{if } q \in \mathcal{C} \text{ for any } x \in \bar{\Omega}, \\ +\infty & \text{if } q \notin \mathcal{C} \text{ for some } x \in \bar{\Omega}. \end{cases} \tag{19}$$

Then we can write the augmented Lagrangian function of (17):

$$\begin{aligned} \mathcal{L}_A(y,c,q,\lambda,\sigma) := &\frac{1}{2}\int_\Omega (J(c,y) - I(x))^2 \mathrm{d}x + \frac{\alpha_1}{2}\int_\Omega \|\Delta y\|_{\mathrm{F}}^2 \mathrm{d}x + \alpha_2 \int_\Omega |k(y)|^2 \mathrm{d}x \\ &+ \int_\Omega \langle \lambda, \nabla^2(\phi \circ y) - q \rangle \mathrm{d}x + \frac{\sigma}{2}\int_\Omega \|\nabla^2(\phi \circ y) - q\|_{\mathrm{F}}^2 \mathrm{d}x + \delta_{\mathcal{C}}(q), \end{aligned} \tag{20}$$

where λ is the Lagrangian multiplier, $\langle \cdot, \cdot \rangle$ is the corresponding inner product and σ is the penalty parameter.

Now by fixing q to solve (y, c) and then by fixing (y, c) to solve q, we can build the k-th iterative scheme of ADMM:

$$\begin{cases} (y^{k+1}, c^{k+1}) & := \operatorname{argmin}_{y,c} \mathcal{L}_A(y, c, q^k, \lambda^k, \sigma); \\ q^{k+1} & := \operatorname{argmin}_q \mathcal{L}_A(y^{k+1}, c^{k+1}, q, \lambda^{k+1}, \sigma); \\ \lambda^{k+1} & := \lambda^k + \sigma(\nabla^2(\phi \circ y^{k+1}) - q^{k+1}). \end{cases} \tag{21}$$

Next, for each subproblem, we first make the discretization to get the corresponding finite dimensional optimization problem and then provide the suitable optimization method. Here, we only consider the 2D case and for the 3D case, it can be implemented just following the same line.

4.1. Discretization

For simplicity, we make the discretization on the image domain $\Omega = [0, 1]^2$ and assume that the target objects are in the interior of the image domain. In the implementation, we employ the nodal grid and define a spatial partition

$$\Omega_h^n = \{x^{i,j} \in \Omega | x^{i,j} = (x_1^i, x_2^j) = (ih, jh), 0 \le i \le n, 0 \le j \le n\},$$

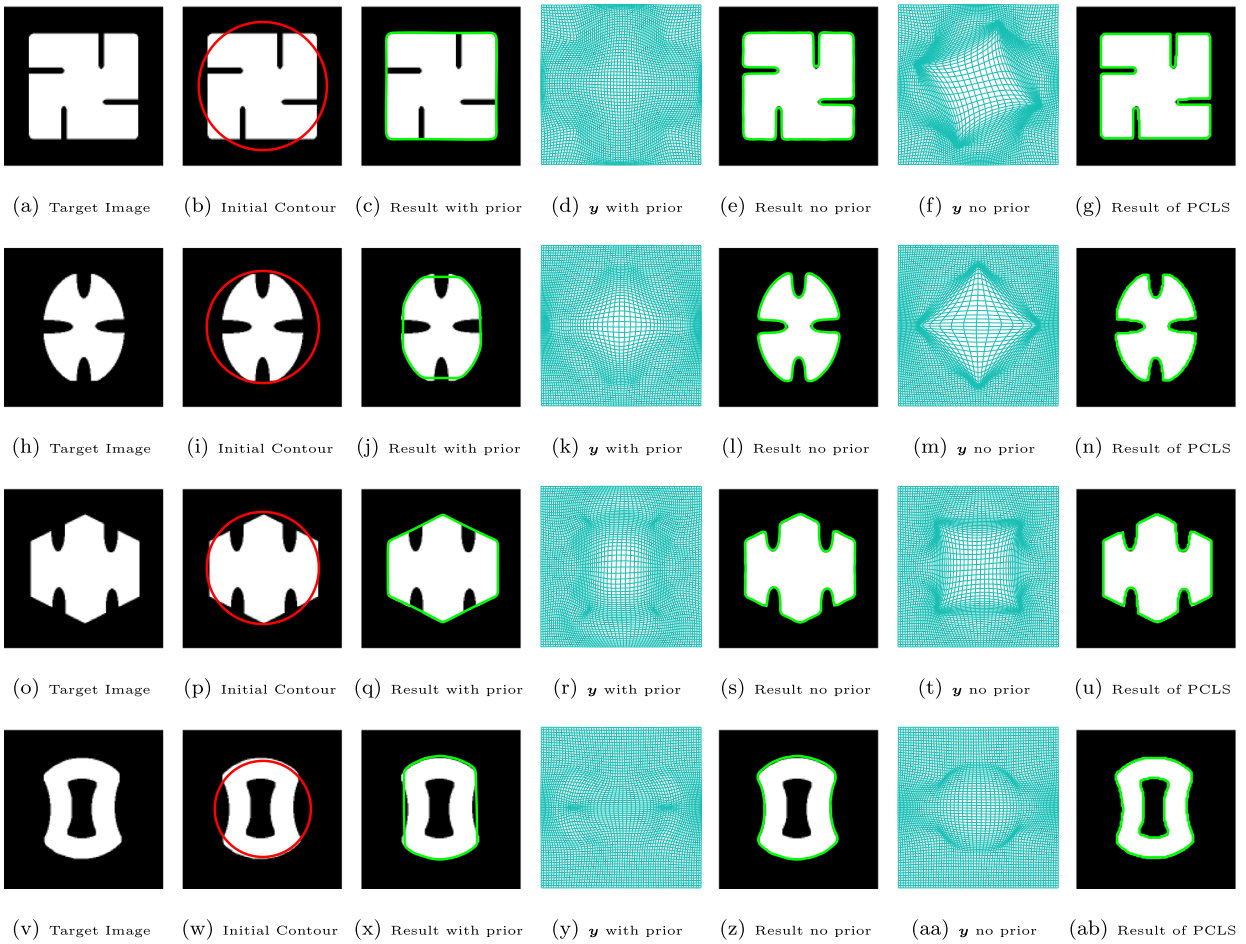

Fig. 1. The first column shows the target images. The second column shows the initial contours. The third and fourth columns give the segmentation results with the convex priors and their corresponding transformations, respectively. For comparisons, the fifth and sixth columns list the segmentation results without the convex priors and their corresponding transformations, respectively. Here, we can see that the proposed model indeed guarantee the topology- and convexity-preserving segmentations. The last column gives the segmentation results by the piecewise constant level set method [9]. Here, we set 2 phase segmentation.

where $h = \frac{1}{n}$. Similarly, the spatial partition of Ω_l, $1 \le l \le m-1$ is defined as

$$\Omega_{lh}^n = \{x^{i,j} \in \Omega_l | x^{i,j,k} = (x_1^i, x_2^j) = (ih, jh), 0 \le i \le n, 0 \le j \le n\}.$$

Then we can discretize y, x, c, ϕ, q and λ and set Y, X, C, Φ, Q and Λ as the corresponding discretizations.

4.2. Subproblem (y, c)

Recall the subproblem (y, c) in (21):

$$\min_{y,c} \frac{1}{2}\int_\Omega (J(c,y) - I(x))^2 dx + \frac{\alpha_1}{2}\int_\Omega \|\Delta y\|_F^2 dx + \alpha_2 \int_\Omega |k(y)|^2 dx + \frac{\sigma}{2}\int_\Omega \left\| \nabla^2(\phi \circ y) - q^k + \frac{\lambda^k}{\sigma} \right\|_F^2 dx. \tag{22}$$

We assume that the intensity values of the discretized image are defined on the cell-centered grid. Hence, we give an averaging matrix P from the nodal grid Y to the cell-centered grid PY [53,54]. Then for the deformed template image $J(c, y)$ and the reference image $I(x)$, we can set $\vec{J}(C, PY)$ and $\vec{I}$ as the corresponding discretized images. For the first part of the regularizer, set the matrix A as the discretized Laplace operator. But for the second part involving the Jacobian determinant $\det \nabla y$, the finite difference discretization cannot guarantee the consistence, which means that the transformation may have foldings but the Jacobian determinant computed by finite difference is positive [54]. To overcome this difficulty, we divide each cell into two triangles and use linear functions to approximate the transformation [41,51].

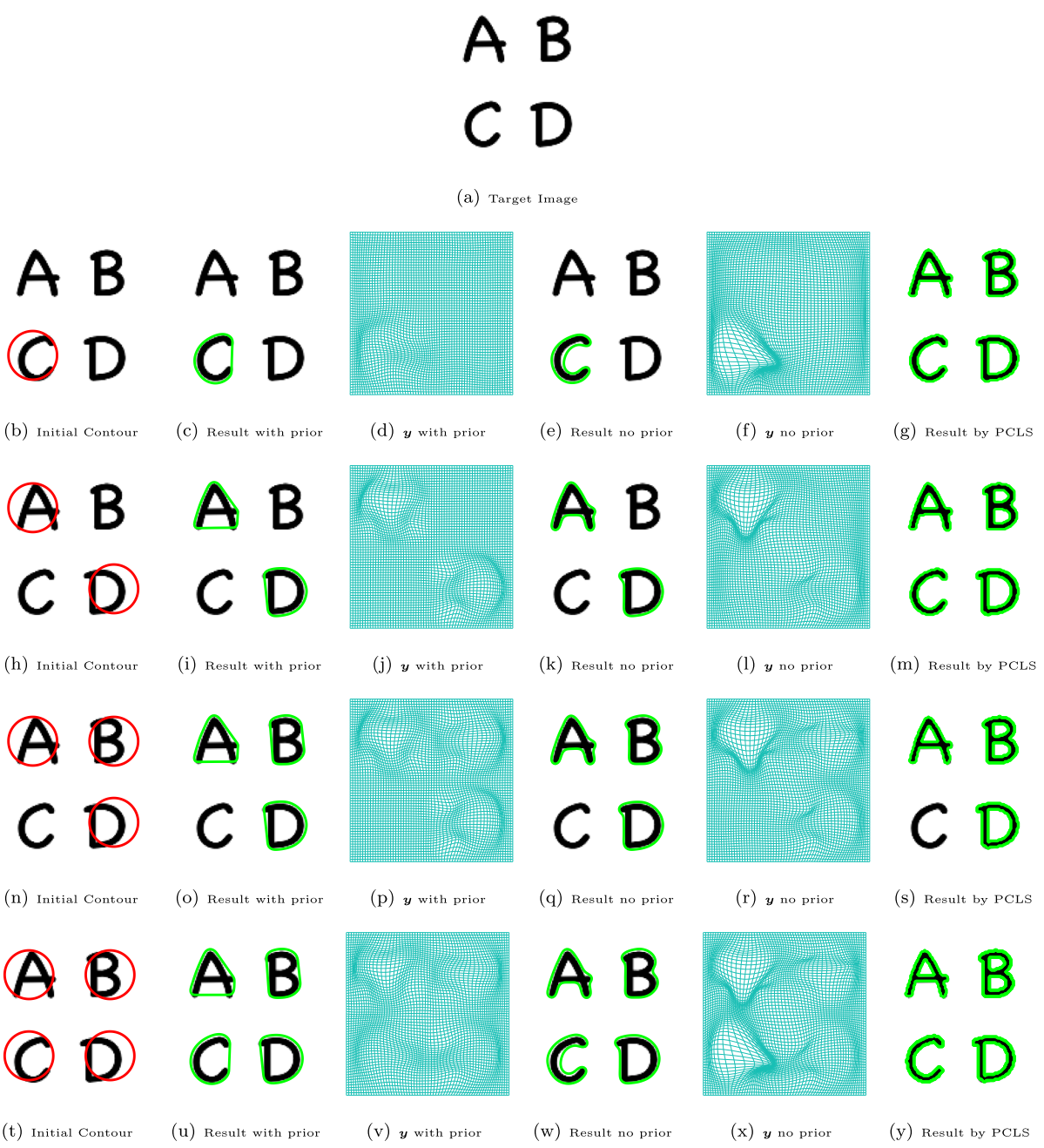

Fig. 2. The target image is displayed in the first row. The first column shows the different initial contours. The second and third columns give the segmentation results with the convex priors and their corresponding transformations, respectively. For comparisons, the fourth and fifth columns list the segmentation results without the convex priors and their corresponding transformations, respectively. Here, we can see that the proposed model can segment the convex target objects by different initial contours. The last column gives the segmentation results by the piecewise constant level set method [9]. Clearly, PCLS is not topology- and -convexity preserving. Here, we set 2–5 phase segmentations, respectively.

Then based on the above discussion, we have the discretized formulation of (22):

$$\min_{Y,C} \frac{h^2}{2}\|\vec{J}(C,PY)-\vec{I}\|_2^2+\frac{\alpha_1 h^2}{2}\|AY\|_2^2+\frac{\alpha_2 h^2}{2}\|K(Y)\|_2^2+\frac{\sigma h^2}{2}\left\|B(\Phi\circ Y)-Q^k+\frac{\Lambda^k}{\sigma}\right\|_2^2, \tag{23}$$

where $K(Y)$ is the discretized conformality distortion and B is the discretized Hessian operator. Here, the implementation of $K(Y)$ just directly follows [41,51] and for the completeness, we give the details in Appendix A.

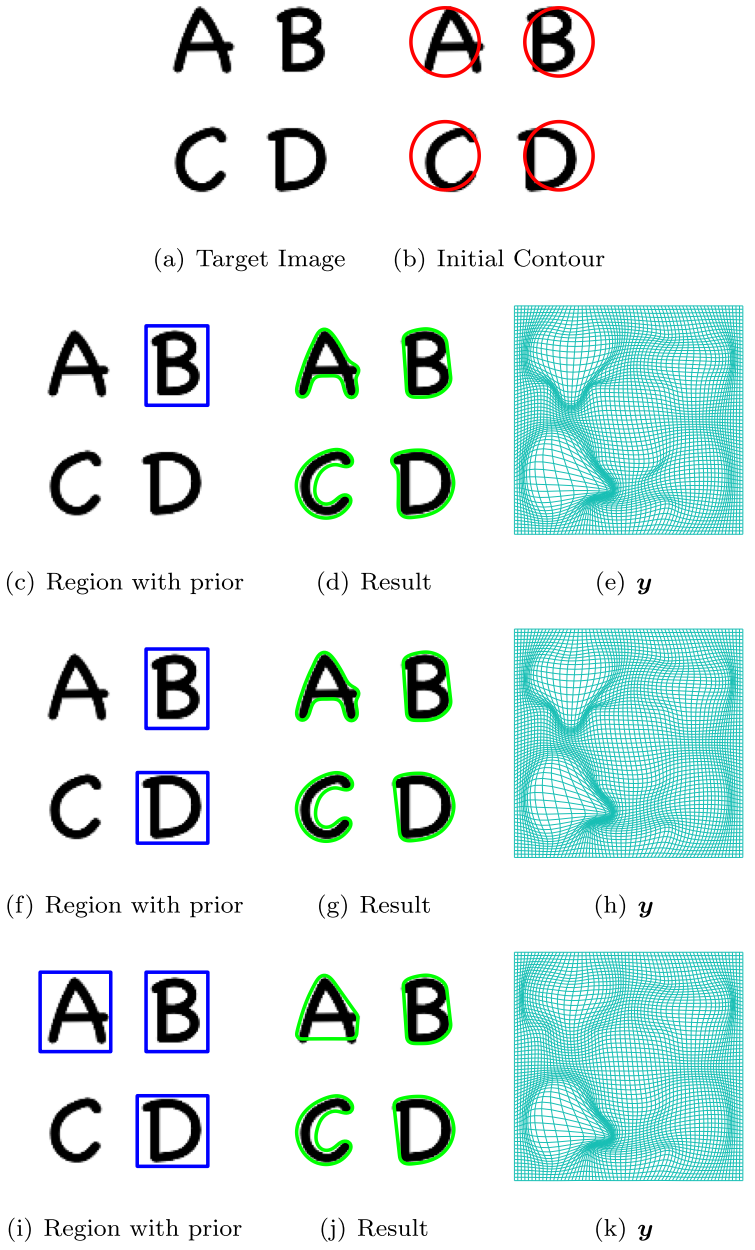

(a) Target Image (b) Initial Contour

(c) Region with prior (d) Result (e) $\boldsymbol{y}$

(f) Region with prior (g) Result (h) $\boldsymbol{y}$

(i) Region with prior (j) Result (k) $\boldsymbol{y}$

Fig. 3. The first row shows the target image and initial contour. The blue boxes in the first column show the region imposing the convex priors. The second and third columns show the segmentation results and the corresponding transformations, respectively. (For interpretation of the references to colour in this figure legend, the reader is referred to the web version of this article.)

To solve (23), since the variables Y and C are coupled, for simplicity, we use the alternating direction method. When we fix Y, C has the following closed-form solution:

$$C_l = \frac{\sum_{y(x^{i,j})\in\tilde{\mathbb{D}}_l} I(x^{i,j})}{\sharp(y(x^{i,j}) \in \tilde{\mathbb{D}}_l)}, \quad 1 \le l \le m. \tag{24}$$

where $\sharp(y(x^{i,j}) \in \tilde{\mathbb{D}}_l)$ denotes the number of points in $\tilde{\mathbb{D}}_l$. When we fix C, we can just use the generalized Gauss-Newton method to solve Y. The key point is to solve the generalized Gauss-Newton system to generate the search direction δY^t:

$$\hat{H}_Y^t \delta Y^t = -g_Y^t, \tag{25}$$

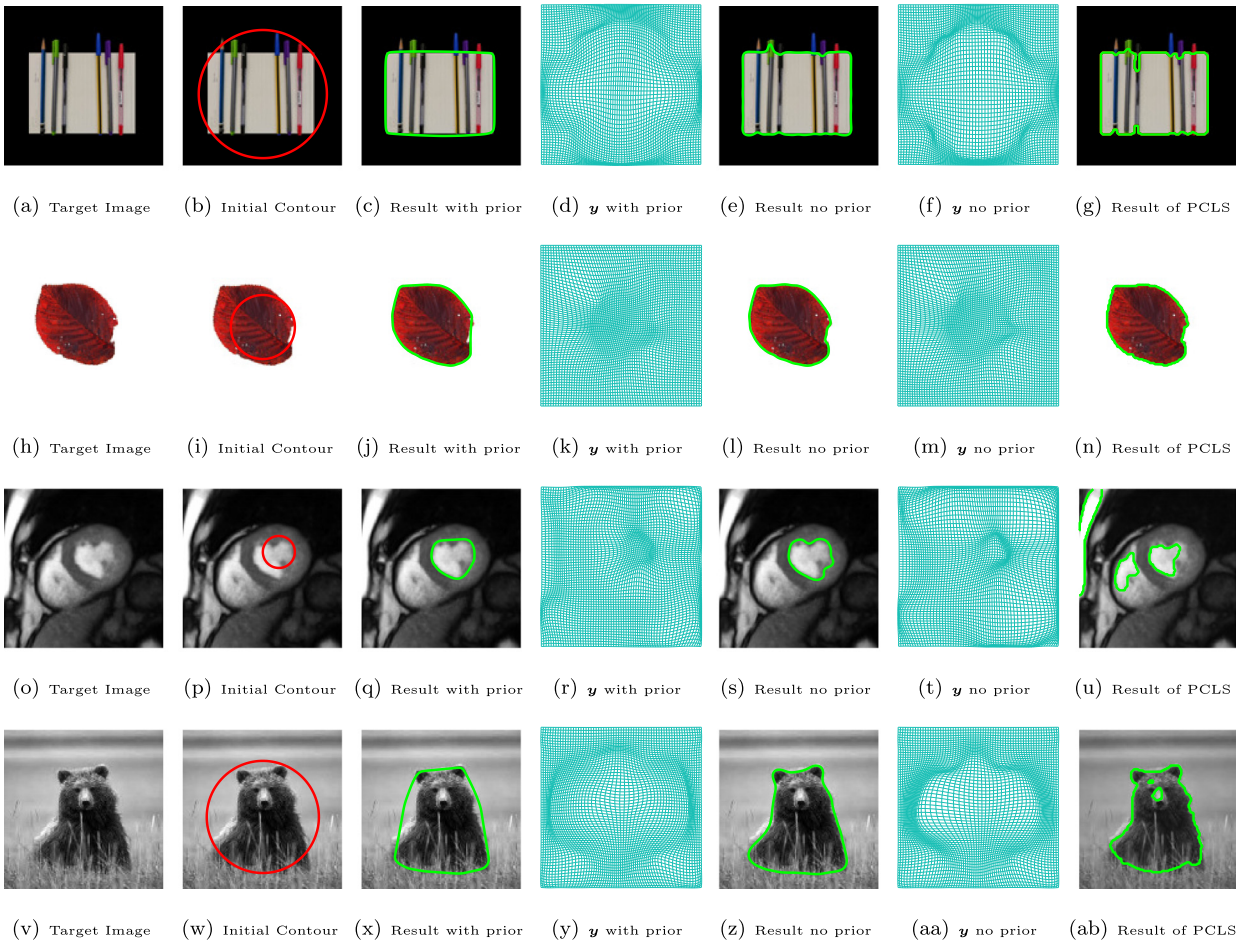

Fig. 4. The first column shows the target images. The second column shows the initial contours. The third and fourth columns give the segmentation results with the convex priors and their corresponding transformations, respectively. For comparisons, the fifth and sixth columns list the segmentation results without the convex priors and their corresponding transformations, respectively. Here, we can see that the proposed model indeed guarantee the convex segmentations. The last column gives the segmentation results by the piecewise constant level set method [9]. Here, we set 2 phase segmentation.

where g_Y^t is the gradient and $\hat{H}_Y^t$ is the approximated Hessian by omitting the second order terms [55], respectively. Specifically, the formulation of g_Y^t and $\hat{H}_Y^t$ are shown in the following:

$$\begin{aligned} g_Y^t &= h^2\left(P^T\vec{J}_{PY^t}^T(\vec{J}(C,PY^t)-\vec{I})+\alpha_1 A^T AY^t+\alpha_2 \mathrm{d}K^T K(Y)+\sigma\,\mathrm{d}\Phi^T B^T(B(\Phi\circ Y^t)-Q^k+\frac{\Lambda^k}{\sigma})\right),\\ \hat{H}_Y^t &= h^2(P^T\vec{J}_{PY^t}^T\vec{J}_{PY^t}P+\alpha_1 A^T A+\alpha_2\mathrm{d}K^T\mathrm{d}K+\sigma\,\mathrm{d}\Phi^T B^T B\mathrm{d}\Phi), \end{aligned} \tag{26}$$

where $\vec{J}_{PY^t}$ is the Jacobian of $\vec{J}$ with respect to PY^t, $\mathrm{d}K$ is the Jacobian of K with respect to Y^t and $\mathrm{d}\Phi$ is the Jacobian of Φ with respect to Y^t. When solving the linear system (25) to obtain the search direction δY^t, we can use Armijo line search to find the step length η_Y^t to update $Y^{t+1}=Y^t+\eta_Y^t\delta Y^t$ [23], which satisfies the sufficient descent condition and simultaneously keeps the discretized Jacobian determinant positive.

Here, we can summarize Algorithm 1 to solve the subproblem (23) when C is fixed.

4.3. Subproblem q

Recall the subproblem q in (21):

$$\min_q \frac{\sigma}{2}\int_\Omega \left\|\nabla^2(\phi\circ y^{k+1})-q+\frac{\lambda^k}{\sigma}\right\|_{\mathrm{F}}^2 \mathrm{d}x+\delta_C(q). \tag{27}$$

By the definition of δ in (19), the discretization of the subproblem (27) is the summation of (27) computed at all discrete grid points. Since this discretization is decoupled with respect to each discrete grid point, it is equivalent to solve some

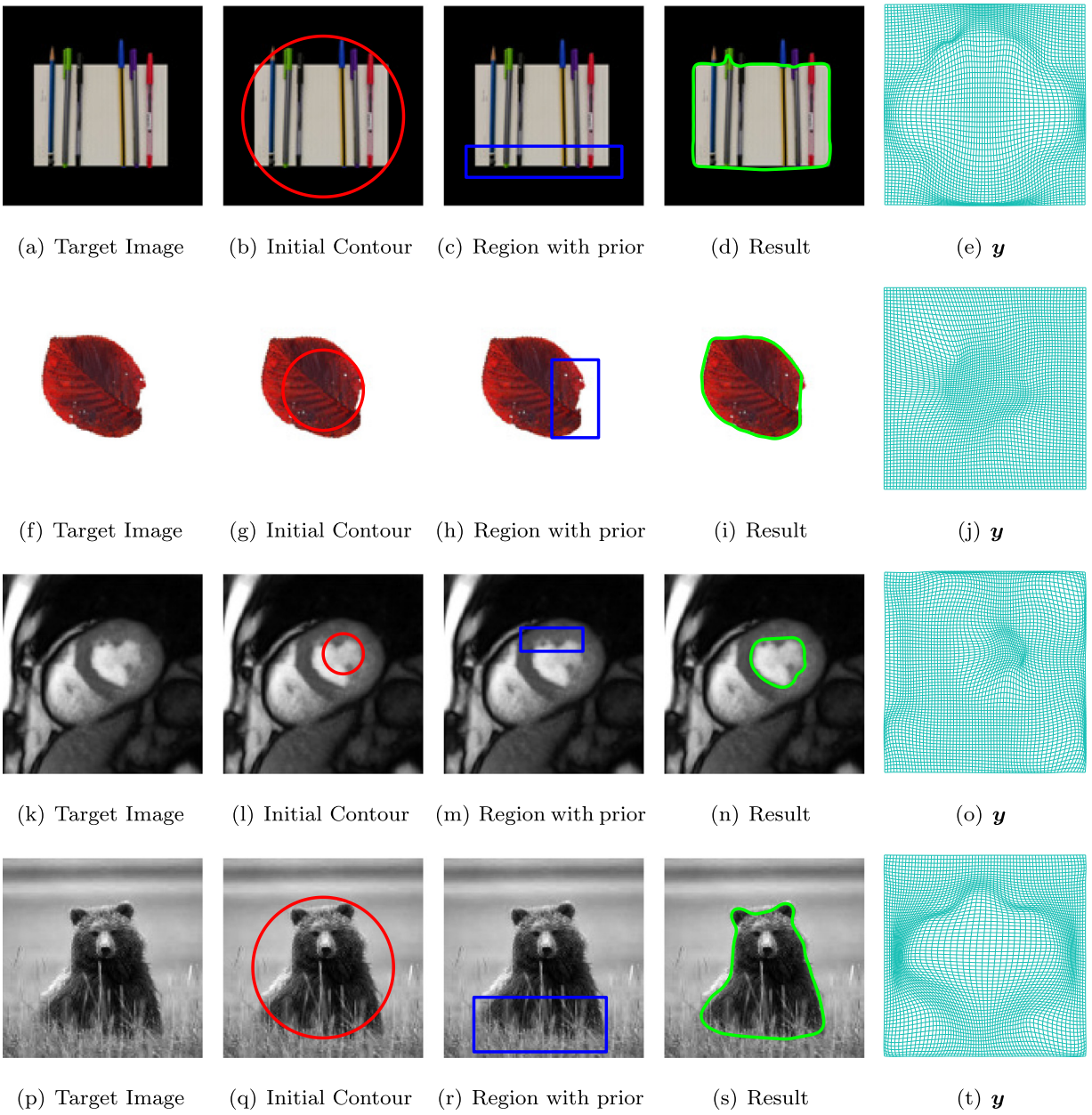

Fig. 5. The first and second columns show the target images and initial contours, respectively. The third column give the partially constraints in the blue boxes. The fourth and fifth columns displays the segmentation results and the corresponding transformations, respectively. Here, we can see that the proposed model allows the partially convex segmentations, which can help to improve the accuracy. (For interpretation of the references to colour in this figure legend, the reader is referred to the web version of this article.)

Algorithm 1 Solve Subproblem (23) when C is fixed to find Y^*.

Set Y^0 and $t = 0$; Compute g_Y^t and $\hat{H}_Y^t$ from (26);
while "stopping criteria is not satisfied" **do**
  Solve $\hat{H}_Y^t \delta Y^t = -g_Y^t$ from (25);
  Update Y^{t+1} by Armijo line search;
  Set $t = t + 1$;
  Compute g_Y^t and $\hat{H}_Y^t$ from (26);
end while

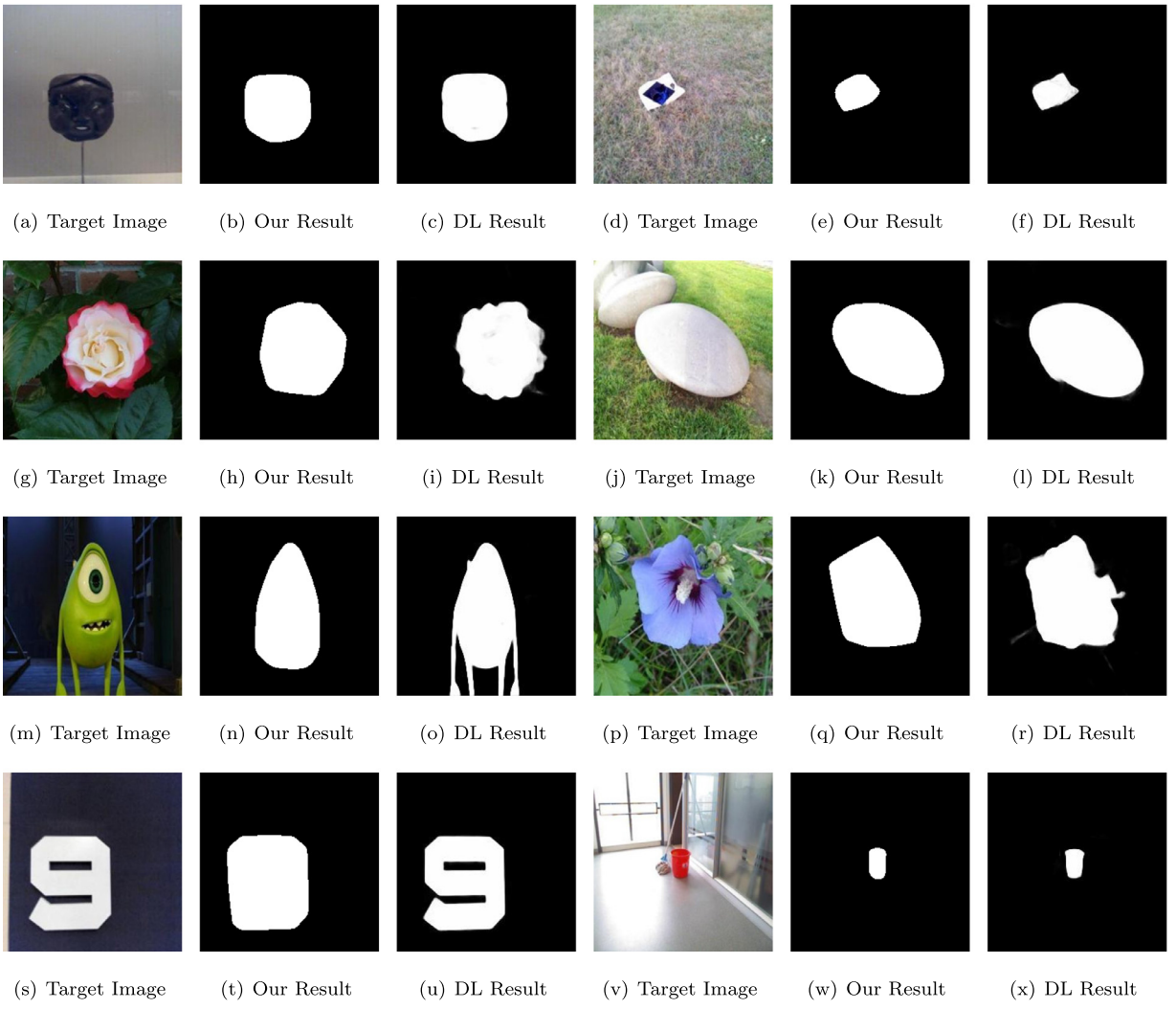

(a) Target Image (b) Our Result (c) DL Result (d) Target Image (e) Our Result (f) DL Result

(g) Target Image (h) Our Result (i) DL Result (j) Target Image (k) Our Result (l) DL Result

(m) Target Image (n) Our Result (o) DL Result (p) Target Image (q) Our Result (r) DL Result

(s) Target Image (t) Our Result (u) DL Result (v) Target Image (w) Our Result (x) DL Result

Fig. 6. The first and fourth columns show the target images. The other columns display the results by our method and [21], respectively.

small optimization problems. Specifically, for each discrete grid point, we have the corresponding closed-form solution:

$$q^*(x^{i,j}) = \begin{cases} \nabla^2(\phi \circ y^{k+1}(x^{i,j})) + \frac{\lambda^k(x^{i,j})}{\sigma}, & \text{for } x^{i,j} \notin \bar{\Omega}, \\ \Pi_{\text{PSD}}\left(\nabla^2(\phi \circ y^{k+1}(x^{i,j})) + \frac{\lambda^k(x^{i,j})}{\sigma}\right), & \text{for } x^{i,j} \in \bar{\Omega}, \end{cases} \tag{28}$$

where Π_{PSD} represents the projection of a matrix into the set of the semidefinite positive matrices. For a 2×2 real symmetric matrix M, its eigenvalue decomposition is $M = UDU^T$, where U is orthonormal and D is a diagonal matrix with all eigenvalues of M on its diagonal entries, namely $D = \text{diag}(d_1, d_2)$. Then by [56], we have

$$\Pi_{\text{PSD}}(M) = UD_{\geq 0}U^T, \tag{29}$$

where $D_{\geq 0} = \text{diag}(\max(d_1, 0), \max(d_2, 0))$ and $\text{diag}(v)$ represents a diagonal matrix with v on its diagonal.

4.4. Numerical implementation of ADMM (21)

Here, combing the above discussions in Section 4.2 and 4.3, we can summarize Algorithm 2 as the numerical implementation of ADMM (21).

Since the suitable choice of σ can significantly affect the convergence [57], here, in Algorithm 2, according to our numerical experience, we simply expand σ by a factor 10 if $\|B(\Phi \circ Y^{k+1}) - Q^{k+1}\|_\infty \geq 0.95\|B(\Phi \circ Y^k) - Q^k\|_\infty$.

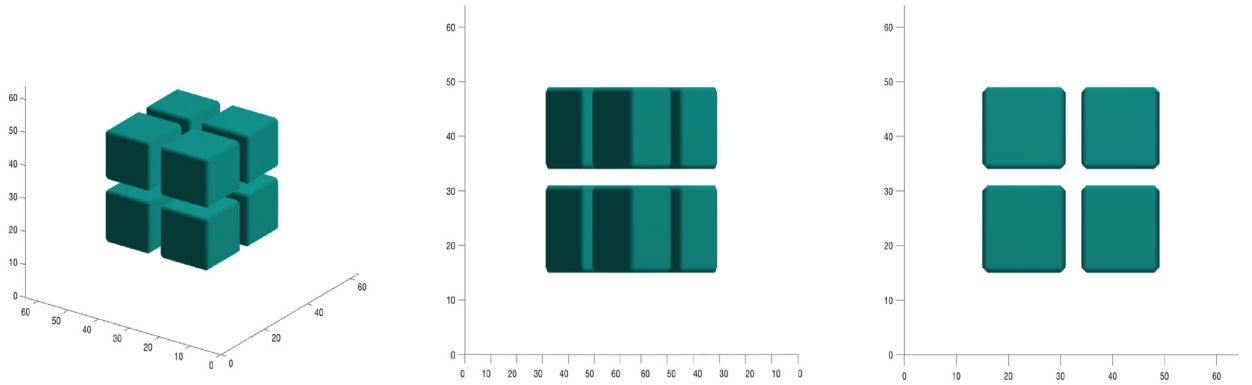

(a) Target Image by different views

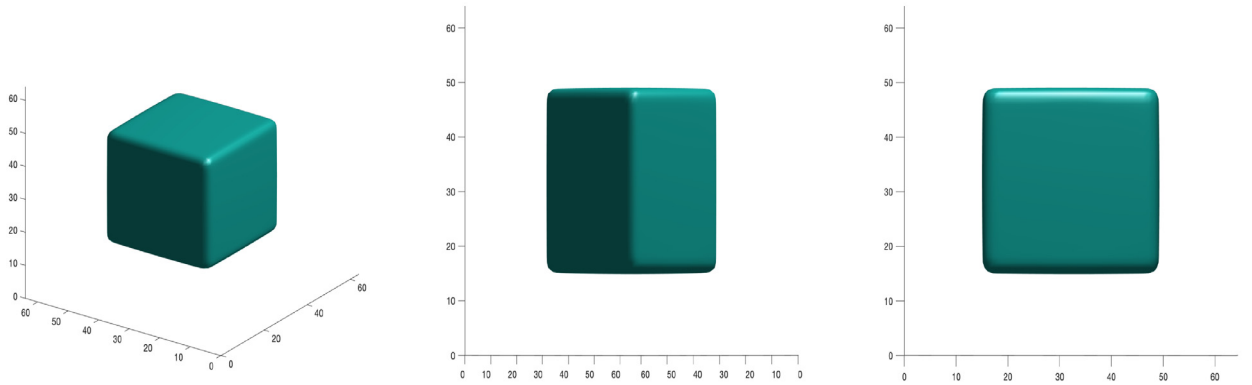

(b) Result with prior by different views

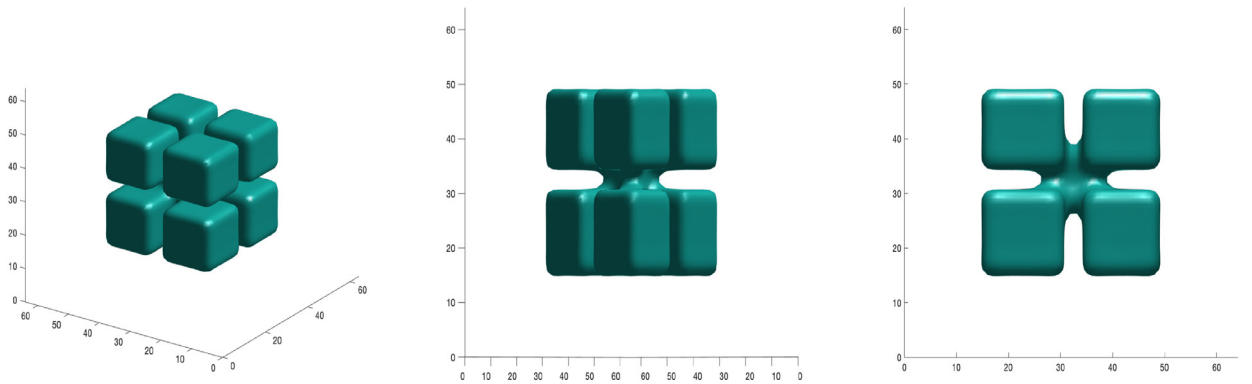

(c) Result without prior by different views

Fig. 7. The first row shows the original volume data. The second and third rows displays the segmentation results with and without convex priors, respectively.

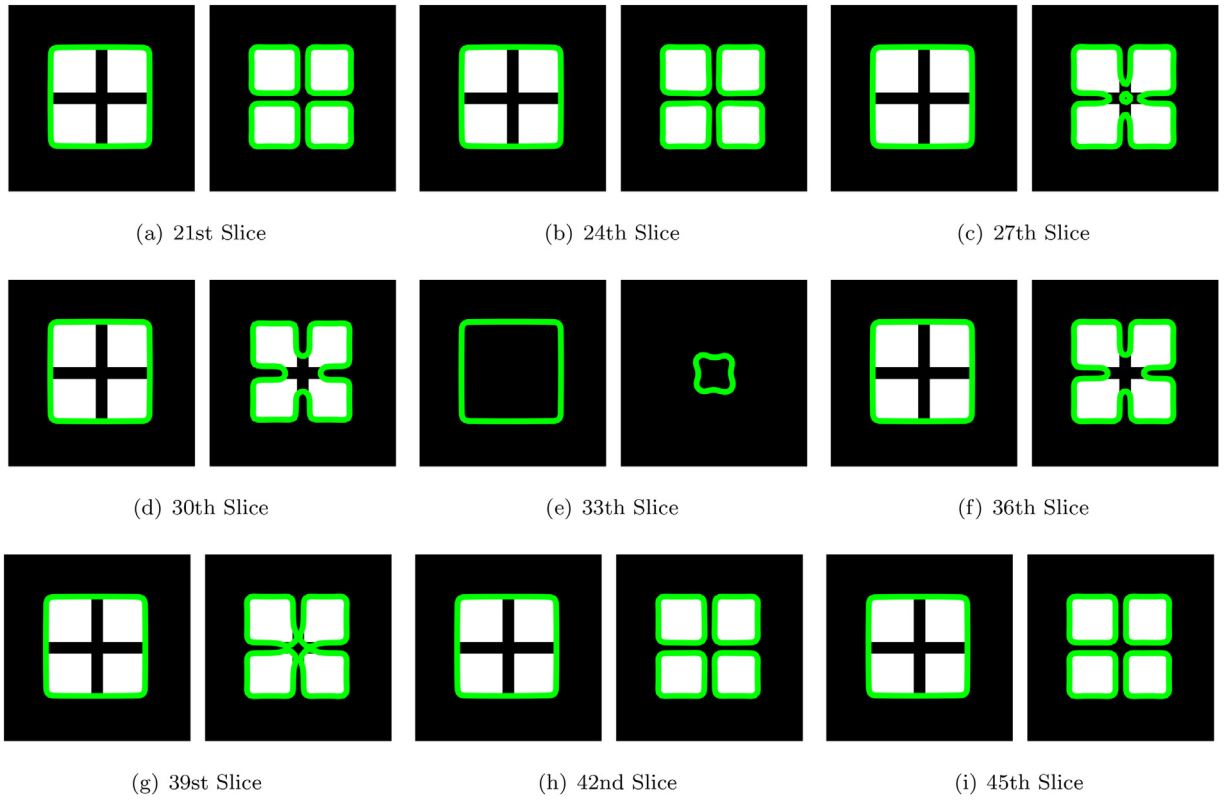

(a) 21st Slice (b) 24th Slice (c) 27th Slice

(d) 30th Slice (e) 33th Slice (f) 36th Slice

(g) 39st Slice (h) 42nd Slice (i) 45th Slice

Fig. 8. Different cross sections of the segmentation results. In each subfigure, the left one is the segmentation result with convex priors and the right one is the segmentation result without convex priors, respectively.

Algorithm 2 Numerical Implementation of ADMM (21) to find C^*, Y^* and Q^*.

Set $k = 0$; Give Y^0, Q^0, Λ^0 and σ^0;
while "stopping criteria is not satisfied" **do**
  Update C^{k+1} by (24);
  Update Y^{k+1} by Algorithm 1;
  Update Q^{k+1} by (28);
  $\Lambda^{k+1} = \Lambda^k + \sigma^k(B(\Phi \circ Y^{k+1}) - Q^{k+1})$;
  if $\|B(\Phi \circ Y^{k+1}) - Q^{k+1}\|_\infty \geq 0.95\|B(\Phi \circ Y^k) - Q^k\|_\infty$ **then**
    Update σ^{k+1} by $\sigma^{k+1} = 10\sigma^k$;
  end if
  Set $k = k + 1$;
end while

5. Numerical results

In this section, we test the proposed model (16) with some synthetic and real images. All codes are implemented by Matlab R2019a on a MacbookPro with 2.2 GHz Quad-Core Intel Core i7 processor and 16 GB RAM. The resolutions of 2D images are 128×128 in Section 5.1 and 5.2 and 224×224 in Section 5.3, respectively. The resolutions of 3D images are $64 \times 64 \times 64$. To make the target object in the interior part, the original data is padded with zero if necessary.

The choice of the parameters is very crucial, especially for a nonconvex model. Here, according to our numerical experience, for the propose model (16), except for the last 3D test, we just set $\alpha_1 = 0.5$ and $\alpha_2 = 10$ and for the last 3D test, we choose $\alpha_1 = 10^{-4}$ and $\alpha_2 = 1$.

5.1. 2D Tests: synthetic images

We first test the proposed model (16) with four synthetic images, which are all simply connected and shown in the first column of Fig. 1. In the second column, we just give a circle possessing the same topology structure with the target images as the initial prior. From the third column, we can see that the proposed model can indeed generate the convex

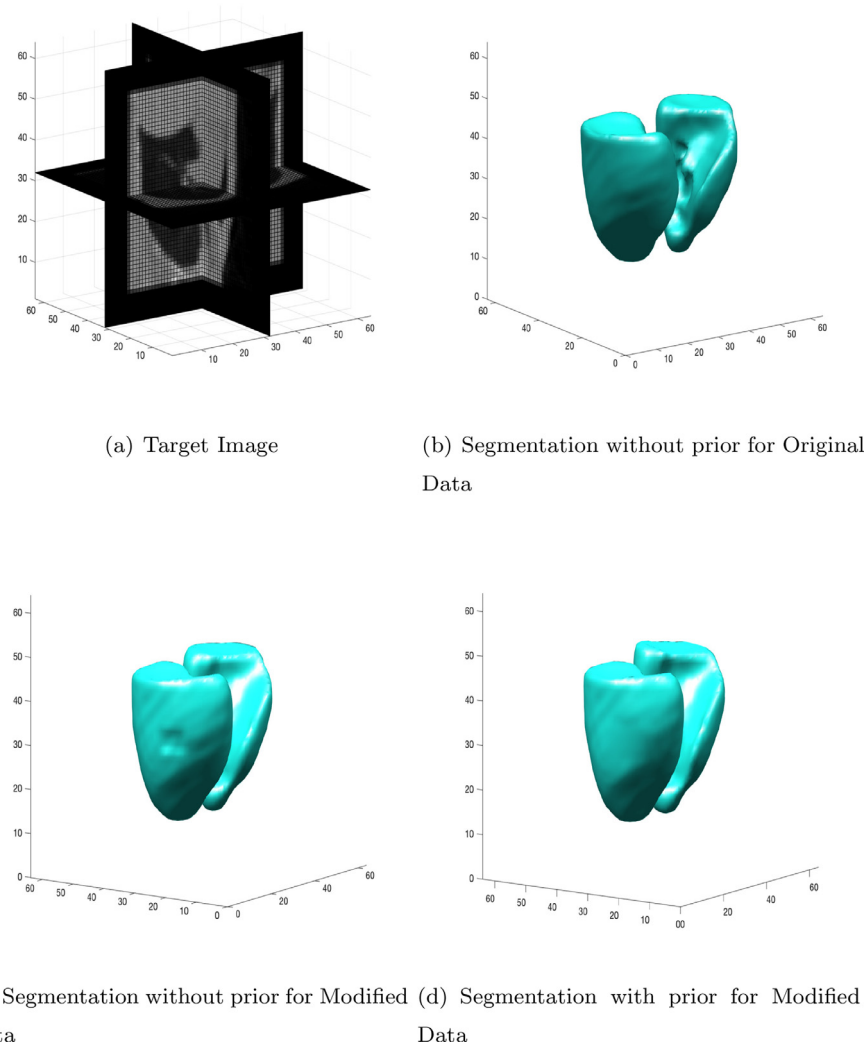

(a) Target Image

(b) Segmentation without prior for Original Data

(c) Segmentation without prior for Modified Data

(d) Segmentation with prior for Modified Data

Fig. 9. The first row displays the original target image and the segmentation result without convex prior for the original data. The second row displays the segmentation result without and with convex prior for the modified data.

segmentations. However, from the fifth column, without the convex priors, the segmented region are not convex. Here, we also plot the resulting transformations with respect to the model with and without convex prior, respectively, displayed in the fourth and sixth columns of Fig. 1. We can see that these transformations are smooth and one-to-one, which means that the segmentations are topology-preserving. We also compare our method with the piecewise constant level set method (PCLS) [9]. The results of PCLS is recorded in the last column of Fig. 1. Here, in the fourth case, it is obvious that PCLS cannot preserve the topology. In addition, it can be observed that the boundaries derived by the registration-based methods are smoother than PCLS because we employ a smooth transformation to deform the initial level set function to locate the boundaries of the targets.

Next, we test the proposed model (16) with an image possessing a more complicated topology structure. The target image shown in the first row of Fig. 2 has four letters. Here, we set four different initial contours. The segmentation results with and without convex priors are shown in the second and fourth columns. We see that the topology structure of these segmentation results is the same with the initial contours', which can be guaranteed by the corresponding transformations. Actually, the minimum of the Jacobian determinant of these transformations are all positive. Further, the proposed model (16) again generates the convex segmentations but without the prior, it will not lead to the convex segmentations. In the last column of Fig. 2, the results of PCLS with different initial contours are listed. Clearly, PCLS is not topology- and -convexity preserving. In addition, although PCLS can define the number of phase manually, it usually cannot locate the desired target. For example, in the first case, since PCLS is not topology-preserving, it segment all the letters as the foreground but the registration-based model can locate the letter "C". Hence, this example illustrates that the proposed model (16) can pick up the specific convex target objects chosen by the users, which is similar to the selective segmentation model.

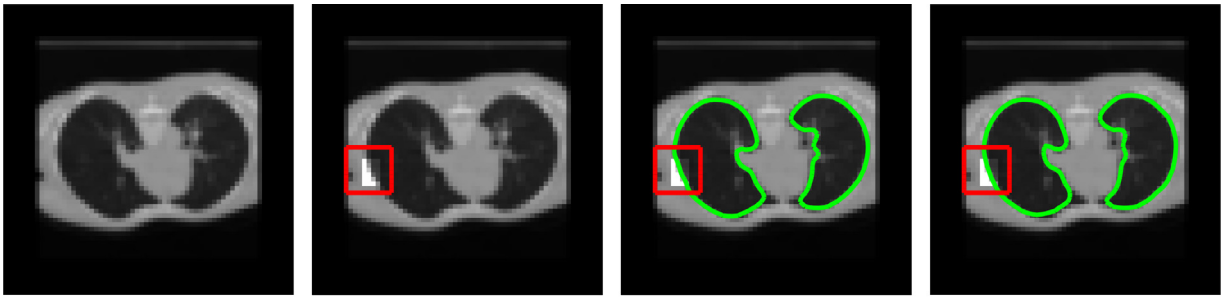

(a) 31st Slice

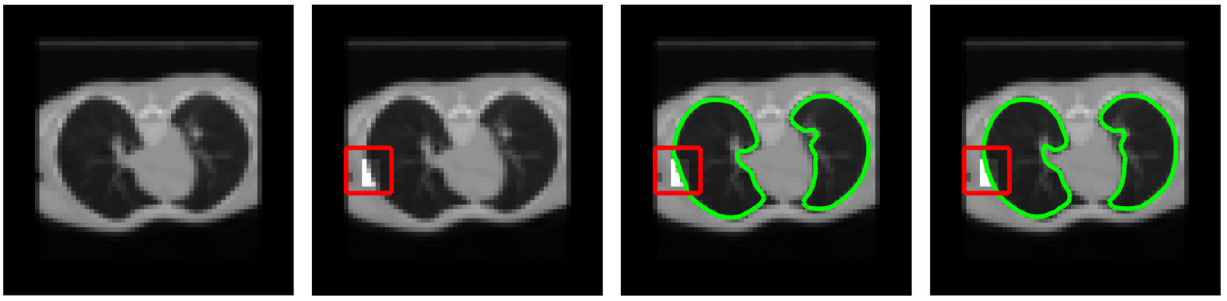

(b) 32th Slice

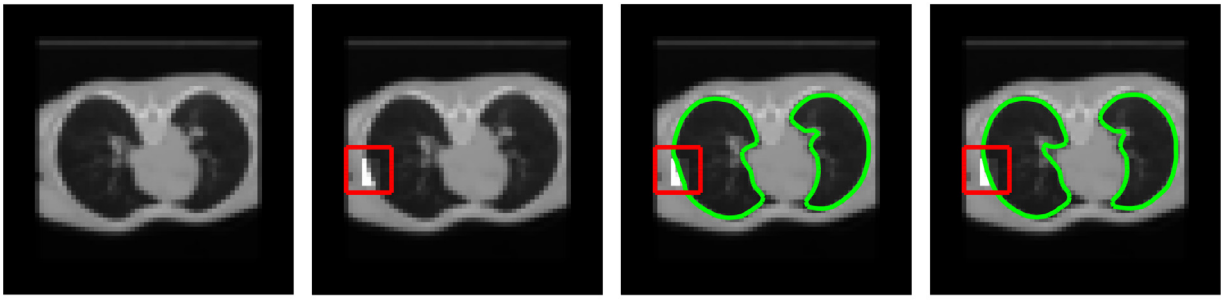

(c) 33th Slice

Fig. 10. In each subfigure, from the left to the right, they are the original data, modified data, segmentation without prior and segmentation with prior, respectively.

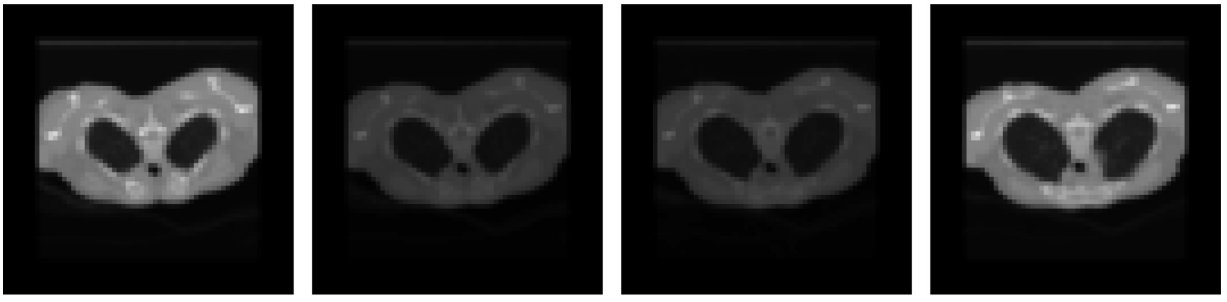

(a) 16th Slice to 19th Slice with underexposure

Fig. 11. Here, we show the 16th Slice to the 19th Slice with underexposure.

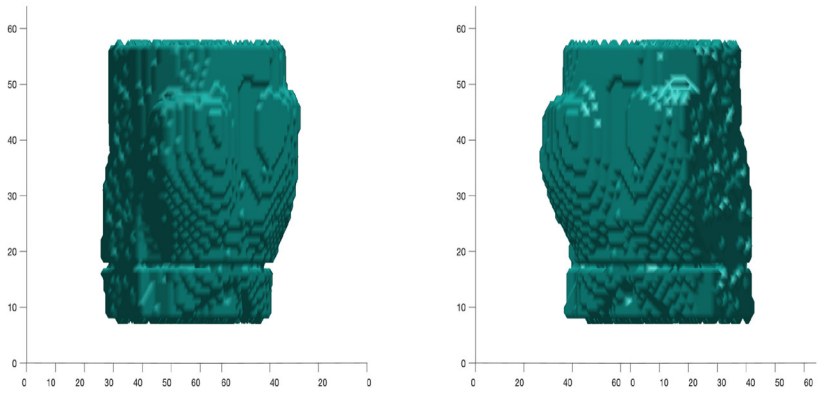

(a) The Chan-Vese segmentation result with underexposure from different views

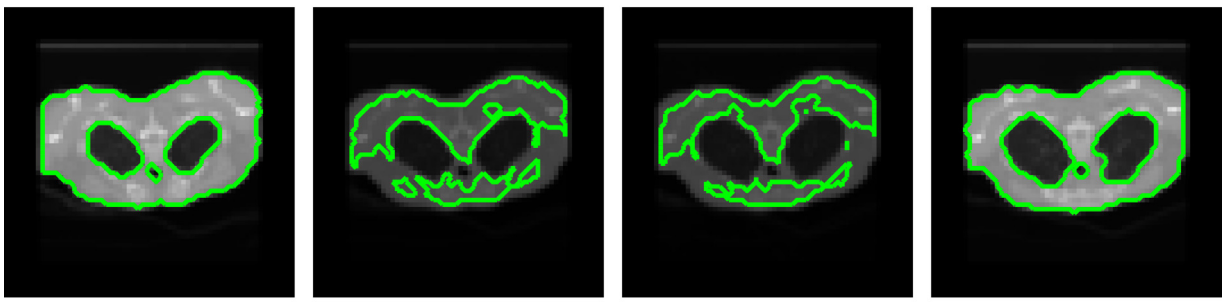

(b) 16th Slice to 19th Slice of the Chan-Vese segmentation result with underexposure

Fig. 12. Here, the first row shows the Chan-Vese segmentation result with underexposure from different views and the second row displays some cross sections of the Chan-Vese segmentation result with underexposure, respectively.

In addition, we also test the partially convex segmentation. In Fig. 3, the target image and initial contour are the same with the fourth case in Fig. 2. But here, we partially impose the constraints in the corresponding blue box regions in the first column. Then from the second column, we can see that the segmentation results only in the regions corresponding to the blue boxes are convex. For the other parts, the segmentations are not convex. This is very flexible for the users to set the desired regions according to the tasks. In addition, although we add the partial constraints, this does not affect the topology-preserving property, which is reflected by the non-folding transformations. Comparing these transformations with the fourth case without convex priors in Fig. 2, we can see that except for the restricted region, the transformations in the other region are almost unchanged.

5.2. 2D Tests: real images

We first test the proposed model (16) with several real images which are shown in Fig. 4. The first and second columns display the target images and the initial contours. The third and fifth columns display the segmentation results with and without convex priors, respectively. Here, it is obvious that with the help of the convex priors, the accuracy of the segmentations can be improved. In addition, the proposed model (16) indeed lead to the topology- and convexity-preserving segmentations. However, for PCLS displayed in the last column of Fig. 4, since it does not preserve the topological structure and convexity, it cannot segment the target object as a whole and the accuracy is reduced.

Furthermore, in Fig. 5, we impose the partially convex priors on the same examples in Fig. 4. And the initial contours are also the same with the cases in Fig. 4. But here, we impose the partially convex priors in the blue boxes shown in the third column and the corresponding segmentation results are shown in the fourth column. It is clear that this kind of priors can significantly help to improve the accuracy. For example, in the second image, the leaf is corrupted and the prior can help to correct this part. In the fourth image, the wild bear with its bottom part is coved by grass and the partially convex prior can help to eliminate this occluded part. As in the synthetic examples, the partially convex priors can be imposed on the target images directly. This is very intuitive by the particular tasks.

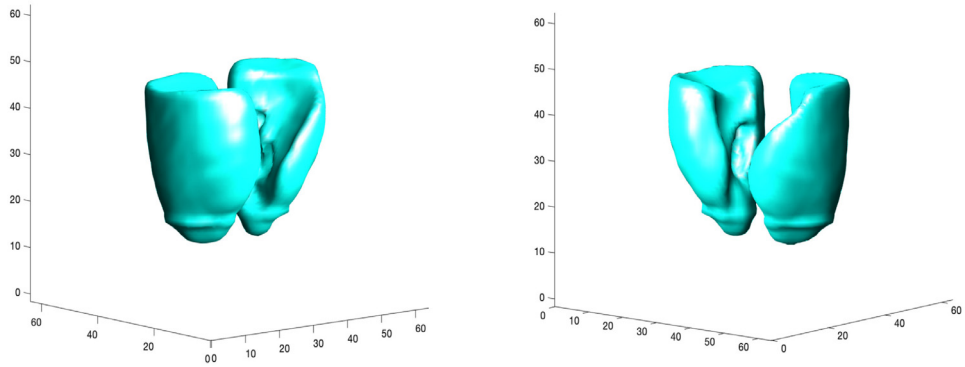

(a) The segmentation result without convex prior for underexposure data

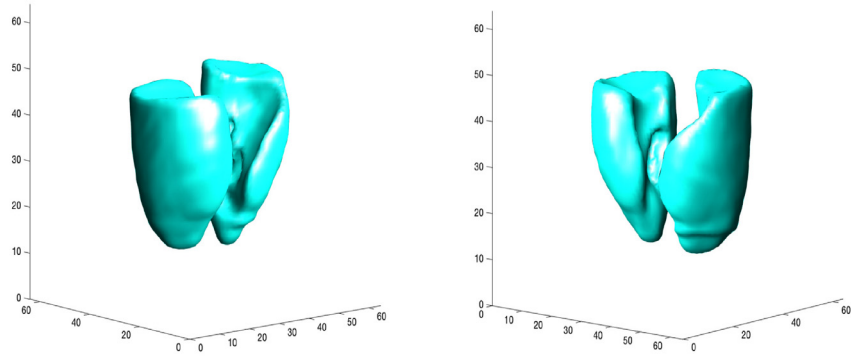

(b) The segmentation result with partial convex prior on the left lung for underexposure data

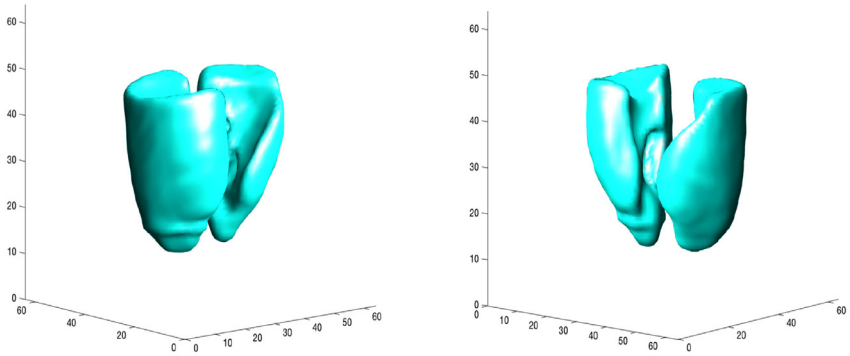

(c) The segmentation result with partial convex prior on the right lung for underexposure data

Fig. 13. Here, the first row gives the segmentation result without convex prior for underexposure data. The second and third rows display the segmentation results by imposing the partial convex prior to the left lung and right lung for underexposure data, respectively.

(a) 16th Slice to 19th Slice with overexposure

Fig. 14. Here, we show the 16th Slice to the 19th Slice with overexposure.

5.3. 2D Tests: Comparison with deep learning method

In this part, we compare the proposed model (16) with one deep learning method [21], which is to extract the salient object for the RGB-D data. The source code and dataset are available and can be downloaded from https://github.com/qdu1995/DQSD. Specifically, we choose eight target images from the dataset displayed in the first and fourth columns of Fig. 6. For our method, we set a disk as the initial prior image. For [21], we simply input the target image into the trained network. The segmentation results by our method (16) and the deep learning method (DL) [21] are shown in Fig. 6. The main difference of these two methods is that our method can give rise to the topology- and convexity-preserving segmentation results, while the deep learning based method cannot. More specifically, the topology of the segmented object is the same as that of the prior image. Also, the segmented object can be constrained to be convex according to user's preference. However, the deep learning method [21] cannot achieve these, since there is no constraint in the network to ensure the topology- and convexity-preserving property.

5.4. 3D Tests: Synthetic images

In this part, we test the proposed model (16) with a synthetic image, which is a cube by removing some parts. The volumetric data is shown in the first row of Fig. 7. Here, the initial contour is a sphere. The segmentation results with and without convex priors are displayed in the second and third rows of Fig. 7. Here, we can see that the segmentation results are topology-preserving, namely, the topology structure of the segmentation results is the same with the topology structure of the sphere. From the second row, the proposed model gives a convex segmentation result. Furthermore, Fig. 8 displays some cross sections of the segmentation results, which also illustrate that the proposed model indeed guarantees the convexity but without the convex constraint, the conventional model can not.

5.5. 3D Tests: real images

Here, we test the proposed model (16) with a real image, which is a lung data downloaded from Dir-Lab (https://www.dir-lab.com). The target image is shown in Fig. 9 (a) and the segmentation result without the convex prior is displayed in Fig. 9 (b), respectively. Here, we just use two separate spheres as the initial guess. With the help of the regularizer, the model can lead to a smooth segmentation result. For simulating the data contaminated by the noise, we artificially change the intensity value of some parts, which is shown in the second column of Fig. 10. If we just apply the registration-based segmentation model without the convex prior to the modified data, from Fig. 9 (c), it is obvious that there is a collapsed part in the lung. However, combining the partial convex prior, we can see that it significantly improves the accuracy of the segmentation result, shown in 9 (d). In addition, the third and fourth columns in Fig. 10 also display several slices of these two segmentation results, which clearly illustrate that the convex prior can help to generate an accurate segmentation result.

To simulate the underexposure case, we rescale the intensity value of the 17th and 18th slice. From Fig. 11, we can see that they are much darker than others. First, we apply the Chan-Vese model, which is implemented by calling the Matlab command "activecontour" with default parameters. The segmentation result is shown in the first row of Fig. 12. Here, we can see that in the bottom part, it is disconnected and since the Chan-Vese model is a global segmentation model, it segments all the objects. To clearly see the interior part, we plot some cross sections of the segmentation results in the second row of Fig. 12, which demonstrate that this segmentation is not topology-preserving and disconnected for the underexposure part. The first row in Fig. 13 shows the segmentation results by the proposed model without the convex prior. It is obviously topology-preserving but for the underexposure part, the segmentation result is not accurate. Further, by imposing the partial convex prior to the left lung and right lung respectively, from the second and third rows in Fig. 13, we can see that with the help of the convex prior, it indeed improves the accuracy of the segmentation.

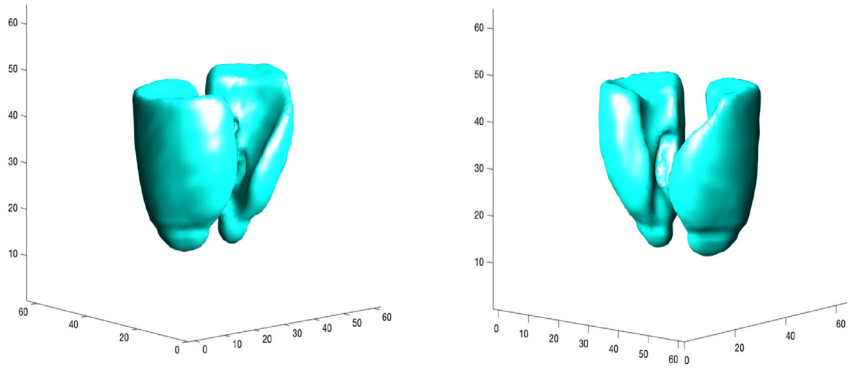

(a) The segmentation result without convex prior for overexposure data

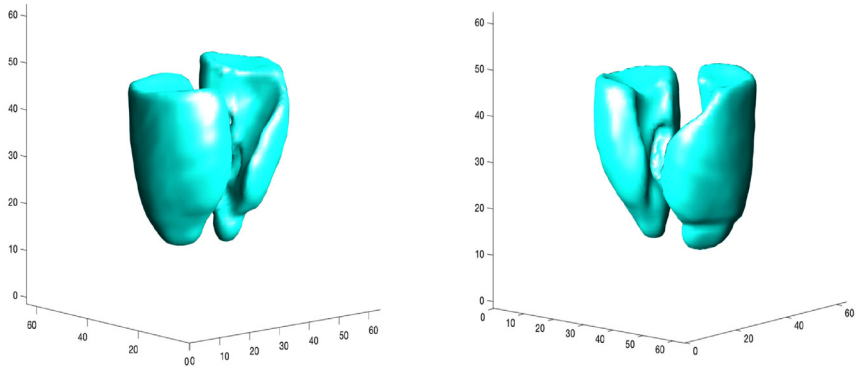

(b) The segmentation result with partial convex prior on the left lung for overexposure data

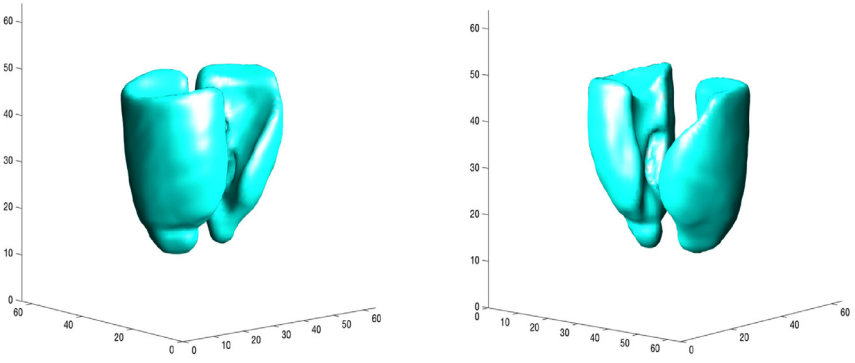

(c) The segmentation result with partial convex prior on the right lung for overexposure data

Fig. 15. Here, the first row gives the segmentation result without convex prior for overexposure data. The second and third rows display the segmentation results by imposing the partial convex prior to the left lung and right lung for overexposure data, respectively.

Table 1
Quantitative measurements of 2D and 3D tests. From this table, we can see that with the help of the regularizer, the model with or without convex prior can lead to a topology-preserving segmentation, because the minimums of the Jacobian determinant of the resulting transformations are all positive.

	With Convex Prior			No Convex Prior		
	Times(s)	$\min \det \nabla y$	$\max \det \nabla y$	Times(s)	$\min \det \nabla y$	$\max \det \nabla y$
2D: Synthetic data in Fig. 1						
Case 1	11.4	0.2230	1.7566	10.2	0.0006	5.7604
Case 2	9.2	0.3502	5.1636	3.9	0.0356	7.6299
Case 3	13.3	0.0502	4.8476	4.1	0.0285	3.4939
Case 4	26.1	0.2250	1.6359	3.2	0.1550	2.2076
2D: Real data in Fig. 4						
Case 1	56.5	0.0044	2.2060	10.1	0.1027	2.1360
Case 2	4.6	0.4077	2.1945	2.5	0.3711	2.0663
Case 3	3.9	0.1084	2.3491	39.8	0.0432	2.8566
Case 4	13.6	0.1390	2.5300	14.7	0.3732	3.6077
3D: Synthetic data in Fig. 7	1148.7	0.2308	3.4156	143.5	0.0558	29.9270
3D: Real data in Figure 9	835.6	0.0056	42.2853	192.8	0.0115	39.8292

Again, to simulate the overexposure case, we rescale the intensity value of the 17th and 18th slice. From Fig. 14, we can see that they are much brighter than others. The first row in Fig. 15 shows the segmentation results by the proposed model without the convex prior. Although it leads to a topology-preserving segmentation result, it has defects in the bottom part. However, with the help of the convex prior, it can eliminate the flaws. Specifically, the second row in Fig. 15 displays the segmentation result with the partial convex prior imposing on the left lung. As the underexposure case, this technique can improve the segmentation result in the restricted region. Similarly, the segmentation result with the partial convex prior imposing on the right lung is shown in the third row of Fig. 15, which also illustrates the advantage of the convex prior. In addition, this convex prior can be added according to the users' preference, which is very flexible.

Finally, we report the quantitative measurements of some 2D and 3D tests in Table 1. Here, again, we can see that with the help of the regularizer in (9), the model with or without convex prior can lead to a topology-preserving segmentation, because the minimums of the Jacobian determinant of the resulting transformations are all positive. For the 2D case, comparing with the model without the convex prior, the computational time of the proposed model (16) is acceptable. But for the 3D case, the computational time is a bit longer and designing a fast solver to speed up the algorithm may be a future work.

6. Conclusion

In this paper, we propose a topology- and convexity-preserving registration-based segmentation model. To ensure the convexity, we incorporate the level set representation with the registration-based model and impose the constraints on the specific regions in the target image, which will lead to the fully convex segmentation or the partially convex segmentation. The selection of the aimed regions is very flexible for the users, according to the specific tasks. To solve the proposed model, we introduce an auxiliary variable and employ ADMM. For the resulting subproblems, one is solved by the generalized Gauss-Newton method and the other one has the closed-form solution. Numerical experiments are carried out on both synthetic and real images, which demonstrates that the proposed model can indeed lead to the accurately topology- and convexity-preserving segmentation.

Acknowledgement

We would like to thank Dr. Hei Long Chan for providing the test images. We would also like to thank Prof. Jan Modersitzki for his FAIR package [39] (https://github.com/C4IR/FAIR.m). Xue-cheng Tai is supported by projects HKBU 12300819, NSF/RGC Grant N-HKBU214-19, ANR/RGC Joint Research Scheme (A-HKBU203-19) and RC-FNRA-IG/19-20/SCI/01. L.M. Lui is supported by HKRGC GRF (Project ID: 2130656; Reference: 14305919) and CUHK Direct Grant (Project ID: 4053292).

Appendix A. Implementation of $K(Y)$

In each tetrahedron $\Omega^{i,j,l}$, set $\mathbf{L}^{i,j,l}(x) = (L_1^{i,j,l}(x), L_2^{i,j,l}(x)) = (a_1^{i,j,l}x_1 + a_2^{i,j,l}x_2 + b_1^{i,j,l}, a_3^{i,j,l}x_1 + a_4^{i,j,l}x_2 + b_2^{i,j,k,l})$, which is the linear interpolation for y in the $\Omega^{i,j,l}$. Note that

$$\partial_{x_1} L_1^{i,j,l} = a_1^{i,j,l}, \partial_{x_2} L_1^{i,j,l} = a_2^{i,j,l}, \partial_{x_1} L_2^{i,j,l} = a_3^{i,j,l}, \partial_{x_2} L_2^{i,j,l} = a_4^{i,j,l}. \tag{A.1}$$

Then we can define the discrete Jacobian determinant in each tetrahedron $\Omega^{i,j,l}$:

$$v^{i,j,l} = a_1^{i,j,l} a_4^{i,j,l} - a_2^{i,j,l} a_3^{i,j,l}. \tag{A.2}$$

Next, we construct D_l, $1 \le l \le 4$:

$$D_1 = [M_1, 0], D_3 = [0, M_1], D_2 = [M_2, 0], D_4 = [0, M_2], \tag{A.3}$$

where M_1 and M_2 are the discrete operators of ∂_{x_1} and ∂_{x_2} respectively and how to construct them is shown in [51]. Then we define $V(Y)$ as follows:

$$V(Y) = D_1 Y \odot D_4 Y - D_2 Y \odot D_3 Y. \tag{A.4}$$

Hence, set $R(Y) = \sum_{l=1}^{4} D_l Y \odot D_l Y$ and we have $K(Y) = R(Y)./(2V(Y))$, where $./$ denotes the component-wise division.

References

[1] A. Elnakib, G. Gimel'farb, J.S. Suri, A. El-Baz, Medical image segmentation: a brief survey, in: Multi Modality State-of-the-Art Medical Image Segmentation and Registration Methodologies, Springer, 2011, pp. 1–39.
[2] W. Khan, Image segmentation techniques: a survey, Journal of Image and Graphics 1 (4) (2013) 166–170.
[3] J.A. Noble, D. Boukerroui, Ultrasound image segmentation: a survey, IEEE Trans Med Imaging 25 (8) (2006) 987–1010.
[4] N.M. Zaitoun, M.J. Aqel, Survey on image segmentation techniques, Procedia Comput Sci 65 (2015) 797–806.
[5] D. Mumford, J. Shah, Optimal approximations by piecewise smooth functions and associated variational problems, Commun Pure Appl Math 42 (5) (1989) 577–685.
[6] T.F. Chan, L.A. Vese, Active contours without edges, IEEE Trans. Image Process. 10 (2) (2001) 266–277.
[7] T.F. Chan, B.Y. Sandberg, L.A. Vese, Active contours without edges for vector-valued images, J Vis Commun Image Represent 11 (2) (2000) 130–141.
[8] T. Chan, B. Sandberg, L. Vese, Active contours without edges for textured images, CAM report (2002) 02–28.
[9] J. Lie, M. Lysaker, X.-C. Tai, A variant of the level set method and applications to image segmentation, Math Comput 75 (255) (2006) 1155–1174.
[10] X.-C. Tai, O. Christiansen, P. Lin, I. Skjælaaen, Image segmentation using some piecewise constant level set methods with mbo type of projection, Int J Comput Vis 73 (1) (2007) 61–76.
[11] T.F. Chan, S. Esedoglu, M. Nikolova, Algorithms for finding global minimizers of image segmentation and denoising models, SIAM J Appl Math 66 (5) (2006) 1632–1648.
[12] M. Kass, A. Witkin, D. Terzopoulos, Snakes: active contour models, Int J Comput Vis 1 (4) (1988) 321–331.
[13] V. Caselles, R. Kimmel, G. Sapiro, Geodesic active contours, Int J Comput Vis 22 (1) (1997) 61–79.
[14] B. Li, S.T. Acton, Active contour external force using vector field convolution for image segmentation, IEEE Trans. Image Process. 16 (8) (2007) 2096–2106.
[15] C. Gout, C. Le Guyader, L. Vese, Segmentation under geometrical conditions using geodesic active contours and interpolation using level set methods, Numer Algorithms 39 (1–3) (2005) 155–173.
[16] N. Badshah, K. Chen, Image selective segmentation under geometrical constraints using an active contour approach, Commun Comput Phys 7 (4) (2010) 759.
[17] M. Roberts, K. Chen, K.L. Irion, A convex geodesic selective model for image segmentation, J Math Imaging Vis 61 (4) (2019) 482–503.
[18] Y. LeCun, B. Boser, J.S. Denker, D. Henderson, R.E. Howard, W. Hubbard, L.D. Jackel, Backpropagation applied to handwritten zip code recognition, Neural Comput 1 (4) (1989) 541–551.
[19] J. Long, E. Shelhamer, T. Darrell, Fully convolutional networks for semantic segmentation, in: Proceedings of the IEEE Conference on Computer Vision and Pattern Recognition, 2015, pp. 3431–3440.
[20] O. Ronneberger, P. Fischer, T. Brox, U-net: Convolutional networks for biomedical image segmentation, in: International Conference on Medical Image Computing and Computer-assisted Intervention, Springer, 2015, pp. 234–241.
[21] C. Chen, J. Wei, C. Peng, H. Qin, Depth-quality-aware salient object detection, IEEE Trans. Image Process. 30 (2021) 2350–2363.
[22] C. Chen, G. Wang, C. Peng, Y. Fang, D. Zhang, H. Qin, Exploring rich and efficient spatial temporal interactions for real-time video salient object detection, IEEE Trans. Image Process. 30 (2021) 3995–4007.
[23] D. Zhang, L.M. Lui, Topology-preserving 3d image segmentation based on hyperelastic regularization, J Sci Comput 87 (3) (2021) 1–33.
[24] H.-L. Chan, S. Yan, L.-M. Lui, X.-C. Tai, Topology-preserving image segmentation by beltrami representation of shapes, J Math Imaging Vis 60 (3) (2018) 401–421.
[25] C.Y. Siu, H.L. Chan, R.L. Ming Lui, Image segmentation with partial convexity shape prior using discrete conformality structures, SIAM J Imaging Sci 13 (4) (2020) 2105–2139.
[26] S. Yan, X.-C. Tai, J. Liu, H.-Y. Huang, Convexity shape prior for level set-based image segmentation method, IEEE Trans. Image Process. 29 (2020) 7141–7152.
[27] E. Strekalovskiy, D. Cremers, Generalized ordering constraints for multilabel optimization, in: 2011 International Conference on Computer Vision, IEEE, 2011, pp. 2619–2626.
[28] L. Gorelick, O. Veksler, Y. Boykov, C. Nieuwenhuis, Convexity shape prior for binary segmentation, IEEE Trans Pattern Anal Mach Intell 39 (2) (2016) 258–271.
[29] E. Bae, X.-C. Tai, Z. Wei, Augmented lagrangian method for an Euler's elastica based segmentation model that promotes convex contours, Inverse Problems and Imaging 11 (1) (2017) 1–23.
[30] S. Luo, X.-C. Tai, L. Huo, Y. Wang, R. Glowinski, Convex shape prior for multi-object segmentation using a single level set function, in: Proceedings of the IEEE International Conference on Computer Vision, 2019, pp. 613–621.
[31] L. Li, S. Luo, X.-C. Tai, J. Yang, A level set representation method for n-dimensional convex shape and applications, Communications in Mathematical Research 37 (2) (2021) 180–208.
[32] M. Sussman, P. Smereka, S. Osher, A level set approach for computing solutions to incompressible two-phase flow, J Comput Phys 114 (1) (1994) 146–159.
[33] J. Nocedal, S. Wright, Numerical Optimization, Springer Science & Business Media, 2006.
[34] S.P. Boyd, L. Vandenberghe, Convex Optimization, Cambridge university press, 2004.
[35] C.R. Vogel, Computational Methods for Inverse Problems, SIAM, 2002.
[36] E. Haber, J. Modersitzki, Intensity gradient based registration and fusion of multi-modal images, in: International Conference on Medical Image Computing and Computer-Assisted Intervention, Springer, 2006, pp. 726–733.
[37] E. Haber, J. Modersitzki, Intensity gradient based registration and fusion of multi-modal images, Methods Inf Med 46 (03) (2007) 292–299.
[38] F. Maes, A. Collignon, D. Vandermeulen, G. Marchal, P. Suetens, Multimodality image registration by maximization of mutual information, IEEE Trans Med Imaging 16 (2) (1997) 187–198.
[39] J. Modersitzki, FAIR: Flexible algorithms for image registration, volume 6, Siam, 2009.
[40] C. Broit, Optimal Registration of Deformed Images, University of Pennsylvania, USA, 1981 Ph.D. thesis.
[41] M. Burger, J. Modersitzki, L. Ruthotto, A hyperelastic regularization energy for image registration, SIAM Journal on Scientific Computing 35 (1) (2013) B132–B148.
[42] G.E. Christensen, R.D. Rabbitt, M.I. Miller, et al., Deformable templates using large deformation kinematics, IEEE Trans. Image Process. 5 (10) (1996) 1435–1447.

[43] N. Chumchob, K. Chen, C. Brito, A fourth-order variational image registration model and its fast multigrid algorithm, Multiscale Modeling & Simulation 9 (1) (2011) 89–128.
[44] M. Droske, M. Rumpf, A variational approach to nonrigid morphological image registration, SIAM J Appl Math 64 (2) (2004) 668–687.
[45] B. Fischer, J. Modersitzki, Fast diffusion registration, Contemporary Mathematics 313 (2002) 117–128.
[46] B. Fischer, J. Modersitzki, Curvature based image registration, J Math Imaging Vis 18 (1) (2003) 81–85.
[47] B. Fischer, J. Modersitzki, A unified approach to fast image registration and a new curvature based registration technique, Linear Algebra Appl 380 (2004) 107–124.
[48] M. Ibrahim, K. Chen, C. Brito-Loeza, A novel variational model for image registration using gaussian curvature, Geometry, Imaging and Computing 1 (4) (2014) 417–446.
[49] Y.T. Lee, K.C. Lam, L.M. Lui, Landmark-matching transformation with large deformation via n-dimensional quasi-conformal maps, J Sci Comput 67 (3) (2016) 926–954.
[50] J. Zhang, K. Chen, Variational image registration by a total fractional-order variation model, J Comput Phys 293 (2015) 442–461.
[51] D. Zhang, K. Chen, A novel diffeomorphic model for image registration and its algorithm, J Math Imaging Vis 60 (8) (2018) 1261–1283.
[52] D. Zhang, K. Chen, 3D orientation-preserving variational models for accurate image registration, SIAM J Imaging Sci 13 (3) (2020) 1653–1691.
[53] E. Haber, J. Modersitzki, Numerical methods for volume preserving image registration, Inverse Probl 20 (5) (2004) 1621.
[54] E. Haber, J. Modersitzki, Image registration with guaranteed displacement regularity, Int J Comput Vis 71 (3) (2007) 361–372.
[55] M. Diehl, F. Messerer, Local convergence of generalized gauss-newton and sequential convex programming, in: 2019 IEEE 58th Conference on Decision and Control (CDC), IEEE, 2019, pp. 3942–3947.
[56] N.J. Higham, Matrix nearness problems and applications, Citeseer, 1988.
[57] S. Boyd, N. Parikh, E. Chu, Distributed optimization and statistical learning via the alternating direction method of multipliers, Now Publishers Inc, 2011.